Rare Metal Materials and Engineering
Volume.50, Issue.4, April 2021
Available online at **www.rmme.ac.cn**

Science Press

Cite this article as: Ding Yutian, Wang Jingjie, Ma Yuanjun, et al. High Temperature Corrosion Behavior of GH3625 Alloy Under Acidic Atmosphere SO_2[J].Rare Metal Materials and Engineering,2021,50(04):1118-1124.

High Temperature Corrosion Behavior of GH3625 Alloy Under Acidic Atmosphere SO_2

Ding Yutian[1,2], Wang Jingjie[1,2], Ma Yuanjun[1,2], Gao Yubi[1,2], Chen Jianjun[1,2], Zhang Dong[3]

[1]State Key Laboratory of Advanced Processing and Recycling of Nonferrous Metals, Lanzhou 730050, China; [2]School of Materials Science and Engineering, Lanzhou University of Technology, Lanzhou 730050, China; [3]State Key Laboratory of Nickel and Cobalt Resources Comprehensive Utilization, Jinchuan Group Ltd, Jinchang 737100, China

Abstract: The corrosion behavior of GH3625 alloy under acidic atmosphere SO_2 at 900 °C was investigated. The surface morphologies of the corroded specimens and the corrosion products were investigated by scanning electron microscopy (SEM), energy dispersive spectroscopy (EDS), and X-ray diffraction (XRD). The cross-sectional morphology was examined by SEM, EDS, and electron probe micro-analyzer (EPMA) to analyze the internal corrosion. The results demonstrate that the corrosion rate of the GH3625 alloy only slightly increases with increasing the SO_2 concentration in the acidic environment. A dense oxide film (primarily Cr_2O_3) forms on the alloy surface which can effectively prevent SO_2 from diffusing into the interior of the alloy matrix. Additionally, chromium inside the matrix can combine with sulfur (primarily CrS) to retard corrosion. GH3625 alloy exhibits excellent corrosion resistance in an SO_2 environment.

Key words: corrosion behavior; SO_2 concentration; high temperature; GH3625 alloy

GH3625 alloy is used to a great extent in the manufacturing of key parts such as gas turbine engines, nuclear power equipment, aerospace engines, and marine applications due to its good oxidation and corrosion resistance properties, as well as good thermal stability and creep strength [1-4]. Various corrosion problems cause great economic losses and security risks. Stress corrosion [5-7] and hot corrosion in molten salts at high temperature [8-11] have been studied extensively, but the investigation of acidic atmosphere corrosion has been rarely studied, especially in pure SO_2 [12-15].

Yang et al [16] investigated corrosion behavior of a new Ni-Cr-Fe base alloy GH984G at 700 °C in a synthetic flue gas environment. A dense protective Cr_2O_3-rich scale forms on the sample surface, leading to good corrosion resistance. Gillot et al [17] studied the corrosion behavior of chromium and manganese in pure SO_2 (890~1350 K, 0.001~0.05 MPa). The duplex sulfide/oxide layer formed during the initial exposure can be explained by the direct reaction of SO_2 with the metal rather than oxygen and sulfur.

In this work, the main objective is to determine the effects of SO_2 concentration on the corrosion mechanism of GH3625. The corrosion tests were performed at 900 °C for 48 h in three gas mixtures (vol%): 2% SO_2/98% Ar, 3% SO_2/97% Ar and 100% SO_2. The results were compared with atmospheric oxidation. Corrosion behavior was studied through mass gain, surface characteristics, and cross-sectional morphology.

1 Experiment

1.1 Material preparation

The main chemical composition (wt%) of the GH3625 alloy used in this study is as follows: 60.63Ni, 21.77Cr, 8.79Mo, 3.75Nb, 3.68Fe, 0.4Ti, 0.21Al, 0.2Mn, 0.19Co, 0.12Si, 0.042C. The 10 mm×10 mm×10 mm specimens were obtained from the original alloy bar by wire electrical discharging machining (EDM). The specimen surfaces were polished with emery papers of 240#, 600#, 800#, 1000#, and 1500# grit sizes, followed by cloth polishing with a buffing compound with a grain size of 0.1 μm. The samples were then cleaned with acetone, ethanol, and distilled water and immedi-

Received date: April 18, 2020
Foundation item: National Key Research and Development Program of China (2017YFA0700703); National Natural Science Foundation of China (51661019); Major Projects of Science and Technology in Gansu Province (145RTSA004); Program for State Key Laboratory of Nickel and Cobalt Resources Comprehensive Utilization (301170503); Hongliu First-class Discipline Construction Plan of Lanzhou University of Technology
Corresponding author: Ding Yutian, Ph. D., Professor, State Key Laboratory of Advanced Processing and Recycling of Nonferrous Metals, Lanzhou University of Technology, Lanzhou 730050, P. R. China, E-mail: dingyt@lut.edu.cn

ately dried with compressed air. Corundum crucibles used in the test were cleaned and heated at 200 °C to a stable weight. The sample-filled corundum crucibles were weighed by a digital weighing balance (DahoMeter FA1004) with 0.0001 mg accuracy.

1.2 Hot corrosion test

Corrosion tests were carried out for 48 h in a chemical vapor deposition furnace (PECVD-12II-3Z/G) at 900 °C with three gas mixtures (volume fraction): 2%SO_2/98%Ar, 3%SO_2/97%Ar, and 100%SO_2 (impurities: O_2<4 μL/L, H_2O<5 μL/L). The contrast specimen was tested at 900 °C in air. First, the samples were placed in the tubular furnace. Next, the furnace was degassed to negative pressure with a vacuum pump. Finally, the furnace was filled with the gas mixture. Heating was conducted under vacuum, and cooling was conducted under pure argon flow.

As shown in Fig. 1, the two gases are charged into the mixing tank at different flow rates, and then the gas mixture is charged into the reaction furnace.

The sample-filled corundum crucibles were cooled to room temperature and weighed. The corrosion rate was determined by the relationship between the mass gain per unit area and the corrosion time in each gas mixture. The surface morphologies of the corroded specimens were investigated with scanning electron microscopy (SEM). The corrosion products were identified BY energy dispersive spectroscopy (EDS) and X-ray diffraction (XRD) with a Cu Kα X-ray source. The specimens were then carefully ground and mechanically polished for cross-sectional observation with SEM and EDS.

2 Results and Discussion

2.1 Corrosion rate analyses

Fig. 2 shows the area specific mass gain ΔM of the GH3625 alloy after 48 h corrosion at 900 °C with different gas mixtures. The samples have a slight mass gain and no serious corrosion when the SO_2 concentration is less than 2%. Even in 100% SO_2 atmosphere, the mass gain is only about 4.5 mg/cm^2. The increase in mass gain indicates that SO_2 accelerates the corrosion of the material. The corrosion rate V_c (V_c=$\Delta M/t$) is calculated by the data in Fig.2, as shown in Table 1. The rate of corrosion increases slightly from 0.2861 g·m^{-2}·h^{-1} in air to 0.3750 g·m^{-2}·h^{-1} in 100% SO_2.

2.2 Surface morphology and phase constitution

2.2.1 XRD analysis

Fig. 3 shows the XRD patterns of the GH3625 alloy before and after the corrosion test under experimental conditions. Fig. 3a shows the XRD patterns of the unprocessed GH3625 alloy, in which the diffraction peaks indicate the presence of only Ni-Cr-Co-Mo. Fig. 3b shows the XRD pattern of the GH3625 alloy after the corrosion tests in different atmospheres at 900 °C for 48 h. The oxidation products of GH3625 alloy in air are primarily Cr_2O_3, $NiCr_2O_4$, and NiO. The highest diffraction peak is Ni-Cr-Co-Mo, and the diffraction peaks of the oxidation products are low, indicating that the oxidation scale is thin. The result also shows that the corrosion products of the GH3625 alloy in gas mixtures with different SO_2 concentrations are similar, mainly Cr_2O_3, NiO, Ni_2S_3, CrS, and a small amount of Nb_2O_5. Neither Al_2O_3 nor TiO_2 were detected from XRD analysis, perhaps owing to their low concentration. The diffraction peaks of Ni-Cr-Co-Mo are still obvious, and the diffraction peaks of the corrosion products are low, showing that the corrosion scale is thin. With increasing the concentration of SO_2, the diffraction peak intensity of Cr_2O_3 increases, indicating that the degree of corrosion increases.

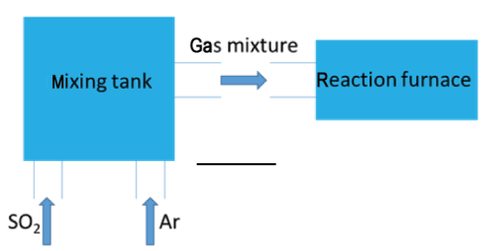

Fig.1 Schematic diagram of gas mixing principle

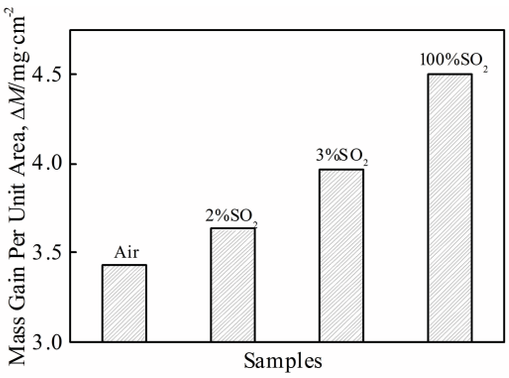

Fig.2 Mass gain of GH3625 alloy corroded in gas mixtures at 900 °C for 48 h

Table 1 Corrosion rate V_c of GH3625 alloy in each gas mixture

Gas mixture	V_c/g·m^{-2}·h^{-1}
Air	0.2861
2%SO_2 + 98%Ar	0.3028
3%SO_2 + 97%Ar	0.3306
100%SO_2	0.3750

2.2.2 Surface corrosion scale characteristics

Fig.4 shows SEM images of the GH3625 alloy after corrosion in different atmospheres at 900 °C for 48 h. As shown in Figs.4a~4d, the alloy shows different features after the corrosion test. Fig.5 shows the EDS analysis of chemical compositions of the surface corrosion of the GH3625 alloy, which shows significant changes at different locations of the corrosion scale.

The SEM plain-view image in Fig. 4a demonstrates that the massive and granular oxide is unevenly and densely distributed on the surface of the oxide scale. On the surface, the corrosion scale (Fig. 4a, point 1) is rich in Cr, Ni, and O, as

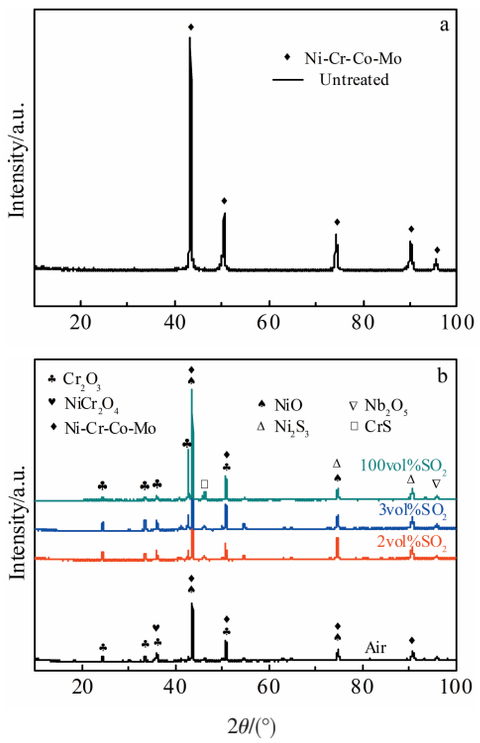

Fig.3 XRD patterns of the GH3625 alloy: (a) unprocessed and (b) corrosion in air, 2% SO_2, 3% SO_2 and 100% SO_2

shown in Fig. 5. XRD analysis confirms that the granule-like oxides are Cr_2O_3 and NiO. At the same time, a larger cellular oxide formed by agglomeration of the granular oxide is observed on the surface of the oxide scale (as shown in point 2 in Fig. 4a). EDS analysis shows a significant increase in Ni concentration and a significant decrease in Cr concentration. XRD analysis shows that the cellular oxide is mainly composed of NiO, $NiCr_2O_4$, and a small amount of Cr_2O_3. It can be concluded that the surface oxidation scale of the alloy is primarily Cr_2O_3, NiO, and $NiCr_2O_4$.

As shown in EDS analysis and Fig.4b~4d, under each experimental condition with SO_2, a dense scale forms on the surface of the alloy. XRD analysis shows that the oxidation scale of the GH3625 alloy in different SO_2 environments is still generally Cr_2O_3 and NiO (as shown in points 3, 4, 6, 8, 10, and 11). However, as shown in Fig. 5b, sulfur can be detected in the corrosion products on the surface of the alloy. XRD results demonstrate that sulfur likely exists as Ni_3S_2 and CrS in the corrosion products (as shown in points 5, 7, 9, and 11).

2.3 Cross-sectional morphology

The corresponding elemental mapping of the GH3625 alloy after oxidation in air is shown in Fig.6, where a thin layer of ~1 μm forms on the surface of the alloy. The scanning results of the cross-sectional mapping (as shown in Fig. 6b~6h) show that the main components in the scale are element Cr and O, which can form Cr_2O_3, and there is a depletion of elemental Mo and Nb. Cr_2O_3 can effectively organize the diffu-

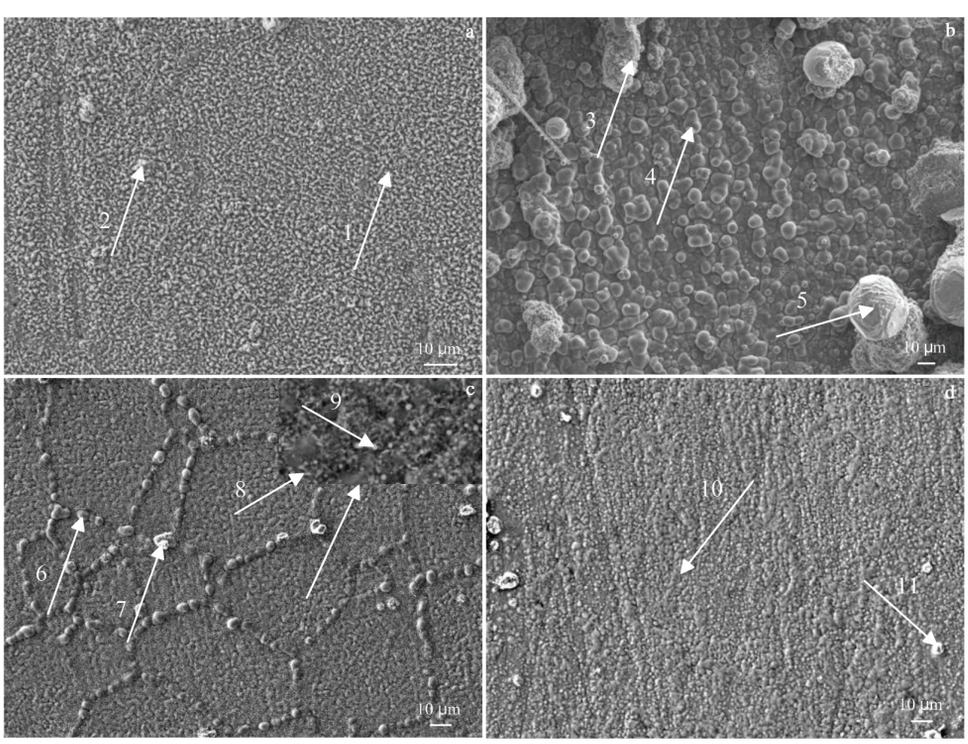

Fig.4 SEM images of GH3625 alloy after corrosion in different atmospheres at 900 °C for 48 h: (a) air, (b) 2% SO_2+98% Ar, (c) 3% SO_2+97% Ar, and (d) 100% SO_2

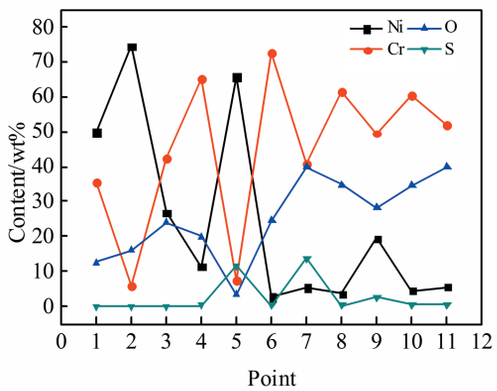

Fig.5 Chemical composition of points marked in Fig.4 of GH3625 alloy after corrosion test

sion of oxygen into the interior of the alloy matrix, as can be-seen from the low distribution of oxygen in the matrix (Fig.6d).

Corrosion severity was also investigated through cross-sectional morphology analysis. Fig.7 shows the cross-sectional morphology images of the GH3625 alloy after corrosion testing. The images show that a thin scale (approximately 0.8 to 2.5 μm) forms on the surface of the alloy with some eroding holes.

Fig.8 shows the line distribution characteristics of the alloy elements of the GH3625 alloy after corrosion, along a direction perpendicular to the interface between the substrate and the scale. As shown in Fig.8, the elements of the surface oxide layer are generally Cr and O. In the vicinity of the contact between the oxide layer and the alloy substrate, the concentration of elemental S and Ni increases. From these data, it can be seen that the thin layer is Cr_2O_3, and that element sulfur can penetrate into the alloy matrix through the oxidation layer.

Fig. 9 shows the cross-sectional EPMA mapping of the GH3625 alloy after corrosion in 2% SO_2. Table 2 shows the EDS results of chemical compositions of the corrosion products of the GH3625 alloy. It is shown that the outer layer is rich in Cr and O and contains a small amount of Ni, Mo and Nb, as shown in Fig.9b~9f and point 1 in Table 2. Combined with XRD data, it is confirmed that it is a layer of Cr_2O_3 with Mo and Nb oxides. The segregation of Mo and Nb is found at the interface between the oxide layer and the alloy matrix. At the same time, Ni and S increase and S extends into the interior of the alloy matrix with approximately the same distribution (as shown in Figs.9e and 9g). In the internal corrosion area, it is found that the two substances are mainly gray and white (as shown in points 2 and 3 in Fig.9a). Combined with EDS analysis results shown in Table 2, compounds in these distribution areas are primarily CrS with a small amount of eutectic Ni-Ni_3S_2, which is consistent with the XRD results in

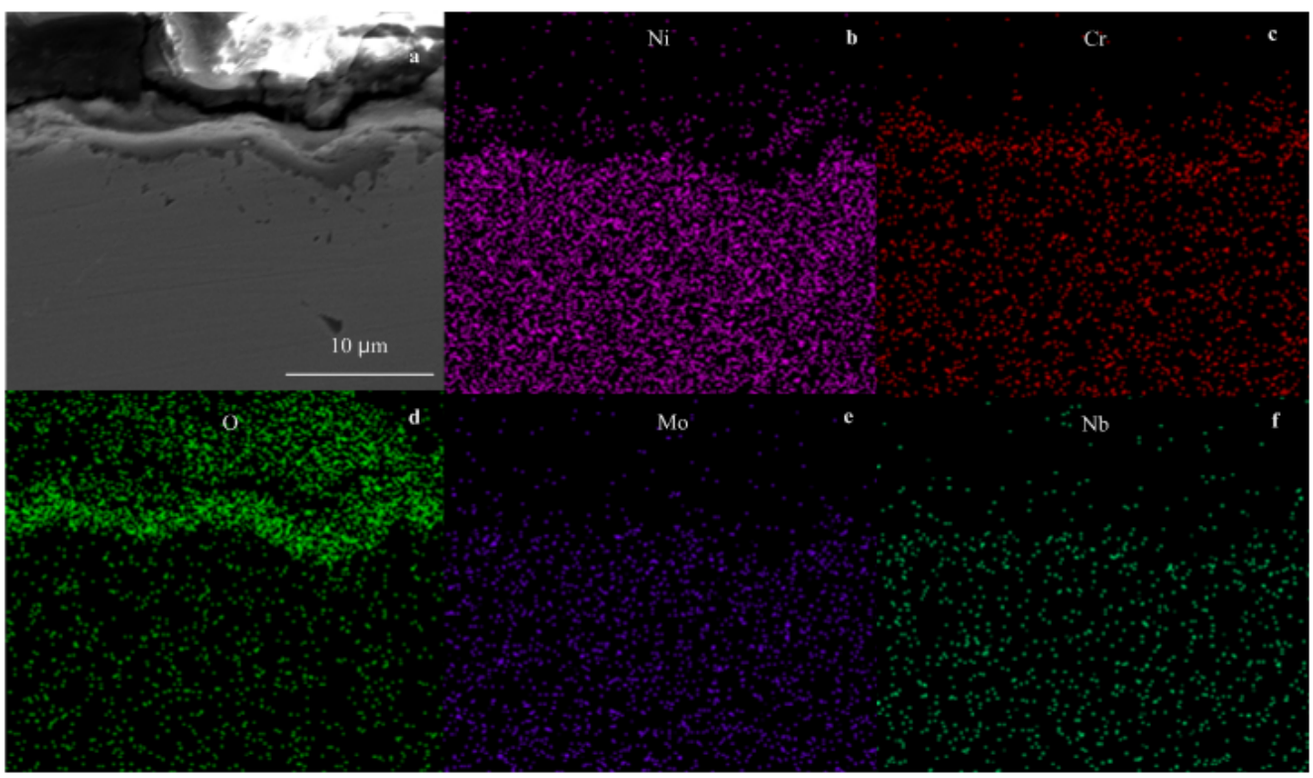

Fig.6 Cross-sectional SEM image (a) and EDS mapping (b~f) of the GH3625 alloy after oxidation at 900 °C for 48 h

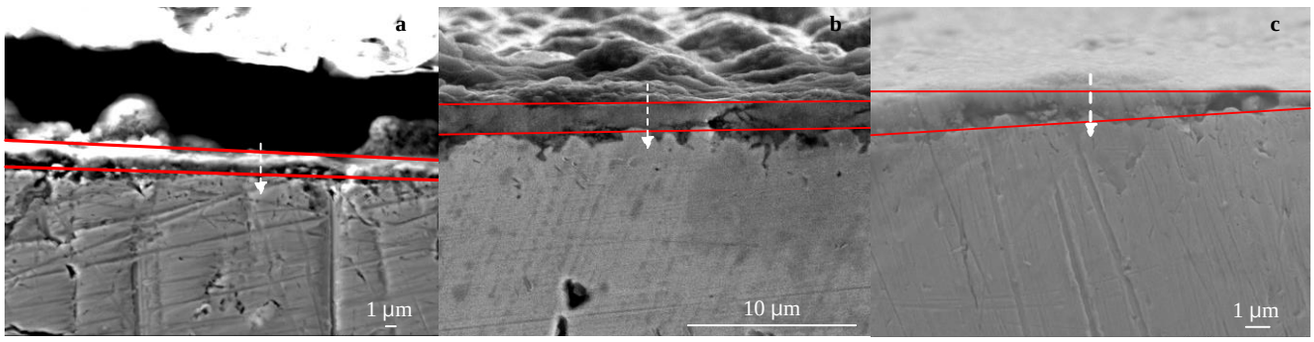

Fig.7 Cross-sectional morphologies of the GH3625 alloy after corrosion testing at 900 °C for 48 h in different environments: (a) 2% SO_2, (b) 3% SO_2, and (c) 100% SO_2

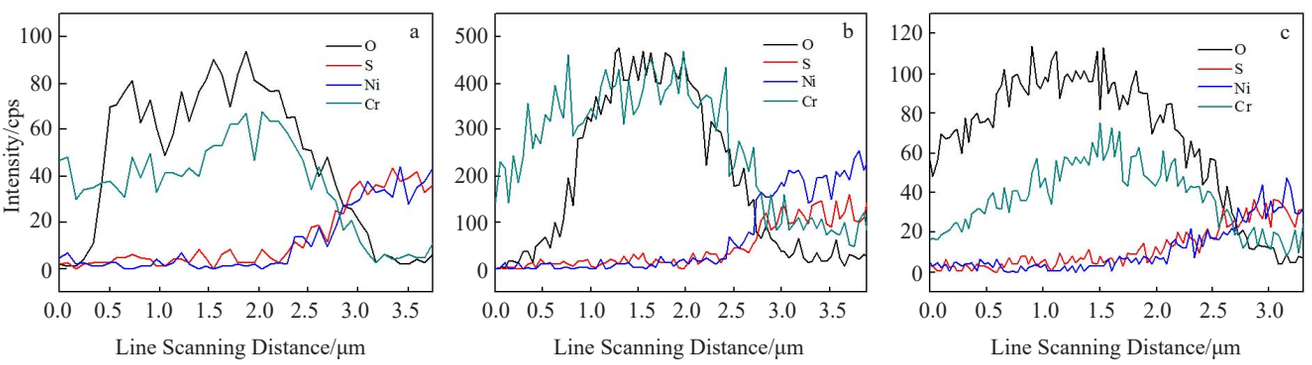

Fig.8 Line scan results of the GH3625 alloy after corrosion testing in different atmospheres at 900 °C for 48 h: (a) 2% SO_2, (b) 3% SO_2, and (c) 100% SO_2

Fig. 3. Although the formation of the Cr_2O_3 layer can protect the substrate from corrosion, sulfur still penetrates the oxide layer and enters the interior of the substrate (as shown in Fig. 9g), which exacerbates alloy corrosion. At point 4 in Fig.9a, it is found through EDS and EPMA results that the element composition here is basically the same as that of the matrix, and no S element or O element is detected, indicating that the corrosion is basically stopped.

2.4 Corrosion mechanism

Alloy oxidation depends on the concentration of a certain element and its Gibbs free energy [18-20]. Based on the analysis of Fig. 6~9, the GH3625 alloy first forms an outer oxide layer of Cr_2O_3 under experimental conditions that contains NiO, a small amount of $NiCr_2O_4$ and TiO_2. From thermodynamic analysis, the Gibbs free energy of Cr_2O_3 is low and the Cr concentration is high, so a layer of continuous and dense Cr_2O_3 film is preferentially formed. Ni has low oxidizing driving force and is oxidized to form NiO, which may react with the Cr_2O_3 solid phase to form $NiCr_2O_4$. Ti has a strong affinity for oxygen, and the outward migration rate is relatively high [21], but the concentration is too low to detect by XRD. When SO_2 and O_2 are present in the simulated flue gas environment, they appear as corrosion of a metal-sulfur-oxygen system, and the formation of oxides is usually accompanied by the formation of sulfides [17]. When the SO_2 concentration is higher than 1%, SO_2 will directly react with metal [22]. Since the concentration of SO_2 in this experimental environment is higher than 1%, the reaction can be performed according to Eq.(1) and Eq.(2). This is consistent with the XRD results in Fig.2b.

$$\frac{7}{2}Cr+\frac{3}{2}SO_2=Cr_2O_3+\frac{3}{2}CrS \quad (1)$$

$$7Ni+2SO_2=4NiO+Ni_3S_2 \quad (2)$$

In the initial stage of corrosion, the surface of the alloy forms a dense Cr_2O_3 oxide scale, so it has better physical resistance to SO_2 penetration and resists the SO_2 corrosion in the alloy matrix [23]. As the experiment progresses, a large concentration of Cr is consumed, forming a Cr-depleted region in the matrix near the oxide film. The Cr concentration is too low to continuously form a dense Cr_2O_3 oxide layer which causes the oxide layer to be weak or defective in the nearby area. Therefore, SO_2 can penetrate into the interior of the matrix through the physical defects in the surface corrosion layer and further form sulfides. Meanwhile, the corrosion rate of metal sulfide is one to two orders of magnitude higher than that of simple oxidation [17]. The main reason is that the defects in the metal sulfide are several orders of magnitude higher than the corre-

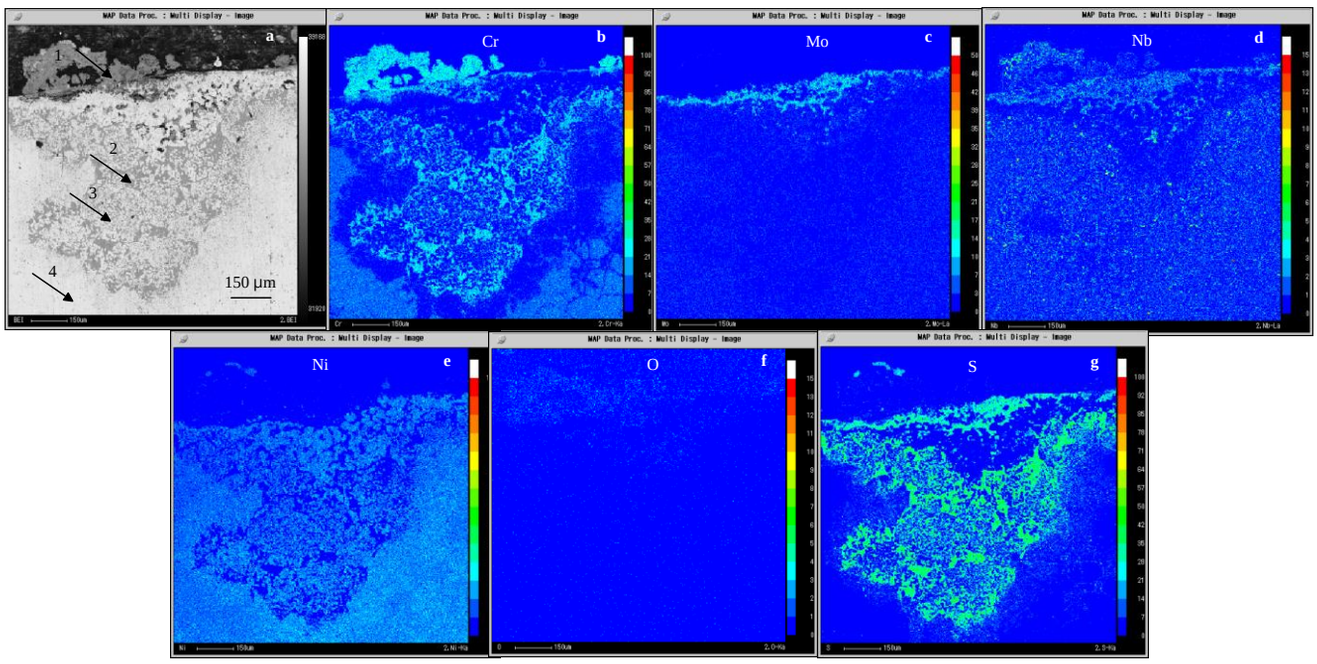

Fig.9 SEM image in backscattered electron mode (a) and cross-sectional EPMA mapping (b~g) of the GH3625 alloy after corrosion in 2% SO_2 atmosphere at 900 °C for 48 h

Table 2 Chemical composition of points marked in Fig. 9a of GH3625 alloy after corrosion test

Point	Ni	Cr	O	S	Mo	Nb
1	3.4	59.2	29.4	2	0.3	5.7
2	4.8	42.7	0.2	47.6	1.5	3.2
3	10.1	42.0	0	42.2	1.9	3.8
4	69.4	20.6	0	0	7.6	2.4

sponding oxides. Therefore, as the SO_2 concentration increases, the corrosion intensifies. According to Gibbs free energy, the thermodynamic driving force of chromium vulcanization is the strongest, and the stability of sulfides is strong, so chromium can preferentially fix sulfur in the form of sulfides (primarily CrS). The element S is fixed, thereby reducing the appearance of eutectic Ni-Ni_3S_2 [24] with a melting point of 645 °C [25]. At 900 °C, the eutectic Ni-Ni_3S_2 will be a molten state, destroying the oxide film and accelerating the alloy corrosion. Therefore, reducing its presence can effectively protect the oxide layer and retard alloy corrosion.

3 Conclusions

1) The degree of corrosion of the GH3625 increases with increasing the SO_2 concentrations.

2) Due to the high concentration of Cr in the GH3625 alloy, a dense Cr_2O_3 oxide layer forms on the surface of the alloy, shielding against penetration by oxygen and sulfur, in different concentrations of SO_2 at 900 °C for 48 h. At the same time, chromium can fix sulfur in the form of sulfide, thereby slowing the corrosion rate of the alloy. Therefore, the GH3625 alloy exhibits excellent corrosion resistance in SO_2 environment.

References

1 Guo Jianting. *Materials Science and Engineering for Superalloys*[M]. Beijing: Science Press, 2008

2 Shankar V, Rao K B S, Mannan S L. *Journal of Nuclear Materials*[J], 2001, 288(2): 222

3 Birn J, Janik-Czachor M, Wolowik A *et al*. *Corrosion*[J], 1999, 55(10): 977

4 Dinda G P, Dasgupta A K, Mazumder J. *Materials Science & Engineering A*[J], 2009, 509(1-2): 98

5 Peng Q J, Kwon J, Shoji T. *Journal of Nuclear Materials*[J], 2004, 324(1): 52

6 Dan T, Shoji T, Lu Z *et al*. *Corrosion Science*[J], 2010, 52(4): 1228

7 WenhaiTuo, Yang Shanglei, Zhang Dongmei. *Rare Metals*[J], 2016, 40(1): 26 (in Chinese)

8 Pradhan D, Mahobia G S, Chattopadhyaym K *et al*. *International Journal of Fatigue*[J], 2018, 114: 120

9 Ye Yun, He Guoqiu, Dai Liquan *et al*. *Metallic Functional Materials*[J], 2016, 23(6): 33 (in Chinese)

10 Khorsand S, Sheikhi A, Raeissi K *et al*. *Oxidation of Metals*[J], 2018, 90(1-2): 169

11 Wang Zhihua, Zhu Ming, Wang Mingjing *et al*. *Rare Metal Materials & Engineering*[J], 2016, 45(3): 677 (in Chinese)

12 Kim M J. *Advanced Materials Research*[J], 2014, 1025-1026: 591

13 Xing Jiandong, Wang Wenhu, Gao Yimin *et al*. *Acta Metallurgica Sinica*[J], 1996, 32(2): 191 (in Chinese)
14 Li Lingchuan, Zhu Rizhang. *Journal of Chinese Society for Corrosion and Protection*[J], 1997(1): 48 (in Chinese)
15 Cao Tieliang, Pan Huiying, Dong Hehua *et al*. *Journal of Chinese Society for Corrosion and Protection*[J], 1994(2): 106 (in Chinese)
16 Yang Huachun, Liang Qin, Yang Xiaochuan *et al*. *Transactions of Materials and Heat Treatment*[J], 2017, 38(1): 83 (in Chinese)
17 Gillot B, Radid M. *Oxidation of Metals*[J], 1990, 33(3-4): 279
18 Li M S. *Metal High Temperature Corrosion*[M]. Beijing: Metallurgical Industry Press, 2001: 248
19 Zheng L, Zhang M, Dong J. *Applied Surface Science*[J], 2010, 256(24): 7510
20 Sidky P S, Hocking M G. *Corrosion Science*[J], 1987, 27(2): 205
21 Abe F, Araki H, Yoshida H *et al*. *Oxidation of Metals*[J], 1987, 27: 21
22 Andersen A G, Kofstad P. *Oxidation of Metals*[J], 1995, 43: 301
23 Birks N, Meier G H, Pettit F S. *Introduction to the High Temperature Oxidation of Metals*[M]. Cambridge: Cambridge University Press, 2006
24 Li Xuefeng, Yang Zhongyuan, Qin Hao *et al*. *Materials Protection*[J], 2002, 35(4): 44 (in Chinese)
25 Zheng X G, Young D J. *Oxidation of Metals*[J], 1994, 42: 163

GH3625合金在SO_2酸性环境下的高温腐蚀行为

丁雨田[1,2]，王靖劼[1,2]，马元俊[1,2]，高钰璧[1,2]，陈建军[1,2]，张　东[3]
(1. 省部共建有色金属先进加工与再利用国家重点实验室，甘肃 兰州 730050)
(2. 兰州理工大学 材料科学与工程学院，甘肃 兰州 730050)
(3. 金川集团股份有限公司 镍钴资源综合利用国家重点实验室，甘肃 金昌 737100)

摘　要：研究了GH3625合金在900 ℃的SO_2酸性环境下的腐蚀行为。通过扫描电子显微镜（SEM），能量色散谱（EDS）和X射线衍射（XRD）研究了腐蚀后试样的表面形态和腐蚀产物。通过SEM，EDS和电子探针微区分析仪（EPMA）检查横截面形态，以观察样品内部的腐蚀。结果表明：GH3625合金在酸性气氛下的腐蚀速率随SO_2浓度的增加而轻微增加。合金表面形成了一层主要是Cr_2O_3的致密氧化膜，该氧化层可以有效阻止SO_2扩散到合金基体内部。另外，基体内部的铬能够以CrS的形式与硫元素结合，减缓腐蚀。GH3625合金在高温SO_2环境中具有优异的耐腐蚀性。

关键词：腐蚀行为；SO_2浓度；高温；GH3625合金

作者简介：丁雨田，男，1962年生，博士，教授，兰州理工大学省部共建有色金属先进加工与再利用国家重点实验室，甘肃　兰州 730050，E-mail：dingyt@lut.edu.cn